J Neurophysiol 102: 3260–3269, 2009.
First published September 2, 2009; doi:10.1152/jn.00663.2009.

Loss of Responses to Visual But Not Electrical Stimulation in Ganglion Cells of Rats With Severe Photoreceptor Degeneration

Chris Sekirnjak,[1] Clare Hulse,[1] Lauren H. Jepson,[1] Pawel Hottowy,[2,3] Alexander Sher,[2] Wladyslaw Dabrowski,[3] A. M. Litke,[2] and E. J. Chichilnisky[1]

[1]*The Salk Institute for Biological Studies, San Diego;* [2]*University of California, Santa Cruz, California; and* [3]*Faculty of Physics and Applied Computer Science, Akademia Górniczo-Hutnicza University of Science and Technology, Krakow, Poland*

Submitted 27 July 2009; accepted in final form 1 September 2009

Sekirnjak C, Hulse C, Jepson LH, Hottowy P, Sher A, Dabrowski W, Litke AM, Chichilnisky EJ. Loss of responses to visual but not electrical stimulation in ganglion cells of rats with severe photoreceptor degeneration. *J Neurophysiol* 102: 3260–3269, 2009. First published September 2, 2009; doi:10.1152/jn.00663.2009. Retinal implants are intended to help patients with degenerative conditions by electrically stimulating surviving cells to produce artificial vision. However, little is known about how individual retinal ganglion cells respond to direct electrical stimulation in degenerating retina. Here we used a transgenic rat model to characterize ganglion cell responses to light and electrical stimulation during photoreceptor degeneration. Retinas from pigmented P23H-1 rats were compared with wild-type retinas between ages P37 and P752. During degeneration, retinal thickness declined by 50%, largely as a consequence of photoreceptor loss. Spontaneous electrical activity in retinal ganglion cells initially increased two- to threefold, but returned to nearly normal levels around P600. A profound decrease in the number of light-responsive ganglion cells was observed during degeneration, culminating in retinas without detectable light responses by P550. Ganglion cells from transgenic and wild-type animals were targeted for focal electrical stimulation using multielectrode arrays with electrode diameters of ~10 microns. Ganglion cells were stimulated directly and the success rate of stimulation in both groups was 60–70% at all ages. Surprisingly, thresholds (~0.05 mC/cm^2) and latencies (~0.25 ms) in P23H rat ganglion cells were comparable to those in wild-type ganglion cells at all ages and showed no change over time. Thus ganglion cells in P23H rats respond normally to direct electrical stimulation despite severe photoreceptor degeneration and complete loss of light responses. These findings suggest that high-resolution epiretinal prosthetic devices may be effective in treating vision loss resulting from photoreceptor degeneration.

INTRODUCTION

The development of retinal prosthetics for the blind has progressed considerably in the past decade. These devices produce artificial vision by electrically stimulating cells that have survived degeneration in diseases such as retinitis pigmentosa (RP). Prototype implants in human patients have produced elementary perception of light and coarse pattern recognition (Mokwa et al. 2008; Winter et al. 2007; Yanai et al. 2007; Zrenner et al. 2009).

An important limitation of existing implants is their large electrode diameter (100–500 μm), which produces nonspecific, simultaneous electrical activation of hundreds or thousands of retinal cells of different types (Mahadevappa et al. 2005). In animal models, significant advances in stimulation specificity have been made by reducing the size of stimulating electrodes, permitting direct activation of one or a few cells (Fried et al. 2006; Jensen et al. 2003; Kuras et al. 2004; Sekirnjak et al. 2006, 2008; Shyu et al. 2006). However, most studies of high-resolution retinal stimulation use healthy animal tissue, whereas degenerated retina exhibits significant changes in cellular architecture, rewired circuitry, and cell hypertrophy resulting from loss of photoreceptors, particularly in non-ganglion cell populations (Jones and Marc 2005; Jones et al. 2003). Recent reports suggest that the morphology (Mazzoni et al. 2008) and membrane properties (Margolis et al. 2008) of ganglion cells in severely degenerated retina remain intact, but do not address responsiveness to extracellular current injection.

Studies of electrical stimulation in degenerated retina have been limited to large-diameter electrodes and/or long pulse durations, which favor activation of bipolar cells and photoreceptors rather than stimulating ganglion cells directly (Fried et al. 2006; Jensen and Rizzo 2008; Margalit and Thoreson 2006). These studies have generally suggested that electrical stimulation in degenerated retina is more difficult than in healthy retina. However, little is currently known about how individual ganglion cells respond to direct, focal electrical stimulation in degenerated retina that has undergone massive remodeling. A better understanding of electrical stimulation in degenerated retina may determine whether implantation in the vitreous cavity provides a promising therapeutic approach (Javaheri et al. 2006).

To examine ganglion cell responses to light and focal electrical stimulation in degenerating retina, we used the pigmented P23H transgenic rat, a model of autosomal dominant retinitis pigmentosa (ADRP). We also used electrical stimulation methods previously shown to directly elicit spiking in ganglion cells with high spatial and temporal resolution. Thus the present work represents the first detailed examination of direct, focal epiretinal stimulation of ganglion cells in degenerated retina. The results indicate that despite complete loss of photoreceptors and light responses, reliable high-resolution stimulation of ganglion cells is possible, with encouraging implications for the design of epiretinal prosthetic devices.

METHODS

Animals and retinal preparation

P23H line 1 homozygous breeding animals (Sprague–Dawley background) were kindly provided by Dr. Matthew LaVail (UCSF School

Address for reprint requests and other correspondence: E. J. Chichilnisky, The Salk Institute for Biological Studies, 10010 North Torrey Pines Rd., La Jolla, CA 92037 (E-mail: ej@salk.edu).

of Medicine, Beckman Vision Center). Line 1 rats have the highest level of P23H transgene expression and show broad similarities to the human ADRP P23H mutation (Machida et al. 2000). The homozygous animals were crossed in our laboratory with pigmented wild-type Long–Evans (LE) rats (Harlan, Indianapolis, IN). The resulting offspring were pigmented P23H heterozygous rats that have a single P23H transgene allele in addition to the normal two wild-type opsin alleles. These heterozygous animals undergo a slower retinal degeneration process than that of homozygous animals and most closely resemble the human genetic condition of RP (a single mutant transgene and two normal copies of rhodopsin). Wild-type LE rats were used as normal controls.

Limited data from three S334Ter rats (line 3) were included in this study for comparison. The animals were kindly provided by Dr. James Weiland (University of Southern California). The S334Ter opsin mutation is a truncation that removes the final 15 amino acids from the carboxy terminus and is representative of a class of RP mutations affecting the cytoplasm-facing end of the rhodopsin molecule (Mendez et al. 2000).

Eyes were enucleated after decapitation of animals deeply anesthetized with 12 mg/kg xylazine and 60 mg/kg ketamine HCl, in accordance with the IACUC of the Salk Institute for Biological Studies for the care and use of animals. Immediately after enucleation, the eye was hemisected about 1 mm behind the ora serrata under infrared illumination. The anterior portion of the eye and vitreous were removed and the eye cup was placed in bicarbonate-buffered Ames' solution (Sigma, St. Louis, MO). The retina was separated from the retinal pigment epithelium by gentle peeling. Pieces 1–2 mm in diameter were cut and placed flat on a multielectrode array (MEA; see following text), with the ganglion cell layer facing the array. A transparent membrane was positioned over the tissue to exert gentle pressure on the preparation. The assembly was then mounted on a circuit board attached to an inverted microscope and continuously superfused with Ames' solution bubbled with 95% O_2-5% CO_2 at a flow rate of 2–4 ml/min (chamber volume 0.4 ml). The tissue chamber temperature was maintained at 30–33°C. In several experiments, the retina was perfused for 5–10 min with cadmium chloride (Sigma), which was dissolved in heated and bubbled bath solution.

The thin and fragile retinas of P23H animals with severe degeneration (>P600) were difficult to separate from the retinal epithelium and sclera for MEA recordings. Thus several of the experiments in older P23H retinas were made using sclera-attached preparations, which allowed for the recording of spontaneous activity, determination of functional cell numbers, and the investigation of responses to electrical stimulation. No systematic differences in the number of functional cells, spontaneous firing rate, or spike amplitude were observed in sclera-attached retinas; thus the data were pooled with those from the remaining experiments.

Multielectrode array

The array, described in detail elsewhere (Litke 1998; Litke et al. 2003; Sekirnjak et al. 2006), consisted of a hexagonal arrangement of 61 extracellular electrodes, used both to record action potentials from ganglion cells and to inject current. Each electrode was formed by microwells that were electroplated with platinum prior to an experiment. Electrode diameter varied between 7 and 16 μm, with a fixed interelectrode spacing of 60 μm. The planar electrode area (πr^2) was used to calculate charge densities. All stimulations were performed using a monopolar configuration (current flow from electrode to distant ground wire).

Electrical stimulation and recording

Stimulation and recording of evoked spikes were performed with custom-designed electronics (Dabrowski et al. 2005). The stimulation pulse consisted of a cathodic (negative) current pulse of amplitude A and duration d, followed immediately by an anodic (positive) pulse of amplitude $A/2$ and duration $2d$. All pulses were calibrated to produce stimuli with zero net charge to minimize electrode corrosion and tissue injury. Pulse durations in this study refer to the duration d of the cathodic phase (either 0.05 or 0.1 ms) and current values refer to the cathodic phase amplitude A. Stimulation frequency was typically 5–10 Hz. Electrical pulses were delivered in darkness.

For each cell, the electrode that recorded the largest spikes was designated as the "primary electrode." All stimulation pulses were delivered through a neighboring electrode on the array, 60 μm away from the primary electrode. This approach significantly reduced the stimulus artifact and avoided amplifier saturation.

Selection of the stimulation site was aided by a map of spike amplitudes surrounding each primary electrode. Since large signals presumably indicate closer proximity to the soma, stimulation was usually attempted using an adjacent electrode with a large spike amplitude. Stimulation was typically commenced by using the lowest available current setting and was then increased systematically if no response was seen. The increase in stimulus amplitude was halted when amplifier saturation and the shape of the stimulus artifact prevented the unambiguous detection of evoked responses. Threshold was defined as the lowest current that produced a spike on 50% of stimulus pulses while stimulating at 5–10 Hz. The exact threshold value was interpolated from several pulse strengths near threshold (for details, see Sekirnjak et al. 2008).

Spontaneous spikes were readily distinguished from evoked spikes since they bore no temporal relationship to the stimulus pulse, whereas evoked spikes were locked to the stimulus onset. Care was taken to match electrically evoked spikes with spontaneous spikes recorded at the primary electrode. This approach ensured that only the responses of a single targeted cell were analyzed.

All submillisecond spike responses were partially obscured by the stimulus artifact. To remove the artifact, several hundred pulses were applied around spike threshold. About half of the pulses evoked spikes whereas the remainder did not. Successes and failures were averaged and subtracted to cleanly reveal the evoked spike. This subtraction method was also used to analyze responses below and above threshold as long as a few traces without evoked spikes were available. A more detailed description of this technique can be found elsewhere (Sekirnjak et al. 2006, 2008).

Latency was defined as the time between the onset of a 0.05-ms pulse and the first unambiguous downward deflection of the voltage signal indicating the evoked spike. In most cells, artifact subtraction yielded distorted or truncated spikes (indicating amplifier saturation); therefore signals from several more distant electrodes were used to align the spike waveforms and accurately determine spike latency at the primary electrode. Latency was measured at response rates close to 50% (near threshold).

Spontaneous firing rates and spike amplitudes

A subset of ganglion cells (between 8 and 17) in each retina were selected for measurement. Electrodes that recorded multiple similar spikes were generally excluded so as not to confound spike counts. Preference was given to cells with medium and large spike amplitudes to facilitate the analysis, but cells with small-amplitude spikes were included if they constituted the only cell recorded at a given electrode. Spontaneous firing rates were measured by counting spikes in 20- to 50-s windows and dividing the number of spikes by the window length. During this time, the cell of interest was not being stimulated electrically and the data were collected in darkness. For each ganglion cell, data from three to four spike-counting periods were averaged. Whenever possible, counting periods interleaved throughout the experiment were used to average out fluctuations in firing rate over time. Spike amplitudes were also measured during these data runs. In animals with very similar ages, spontaneous rate data were pooled and assigned to an average age. For statistical analysis, the firing rates at

each P23H time point were compared with those of wild-type control animals of a similar age.

Light responses and ganglion cell counts

Details of the visual-stimulation technique are given elsewhere (Chichilnisky 2001; Litke et al. 2003; Sekirnjak et al. 2008). Briefly, an optically reduced dynamic checkerboard (white noise) stimulus from a computer display was focused on the photoreceptor outer segments. The voltage signal on each electrode during the stimulus presentation was digitized at 20 kHz and stored for off-line analysis (for an in-depth description of the recording and spike-sorting methods, see Litke et al. 2004). Data were collected continuously during several 30-min periods before and after electrical stimulation. The visual stimulus consisted of a lattice of randomly flickering bright colored pixels (photopic light levels) updated every 16–24 ms. Reverse correlation produced a spike-triggered average (STA) stimulus for each cell. At each spatial location within the STA, the correlation between stimulus and response was declared significant if the time course of the red, green, or blue display primary in the STA exceeded 3 SDs above the average. This definition was used to identify about 90% of light-responsive cells in the preparation. The remainder were inspected manually and cells were classified as non-light-responsive if they lacked an unambiguous peak in the 300 ms preceding a spike.

Ganglion cells were counted within each separate period of visual stimulation. Each such period typically yielded about 25–40 distinct cells; cumulative cell counts across two to three periods yielded about 40–55 unique ganglion cells. This methodology was applied to data from both control and degenerated retina.

Retinal thickness assessment

About a third of retinas measured came from animals also used for electrophysiological recordings and stimulations (in these animals, one eye was used for histology and the other for physiological experiments). Eyes were enucleated and vitrectomies performed as described earlier, followed by immersion in 4% paraformaldehyde for a minimum of 30 min. Each retina was cut into four quadrants and separated from the retinal pigment epithelium. The quadrants were immersed in a concentrated solution of Azure B for several seconds, then separated into central and peripheral portions. Flattened pieces of retina were dissected transversely with a Valet razor blade to produce thin transverse slices. Following a second brief application of Azure B, the slices were positioned with their cut surfaces facing the bottom of a glass petri dish and imaged from below using an Olympus inverted microscope under transmitted white light.

Measurements of retinal thickness were made from 10 to 30 images of retinal slices from each animal. The entire extent of the retina was measured from the inner limiting membrane to the photoreceptor outer segments. Measurements of the photoreceptor layer included only the outer nuclear layer, inner and outer segments. The 10–30 measurements were averaged to provide a single value for each animal. Slices encompassed both central and peripheral locations and included the dorsal, temporal, and ventral quadrant of each retina. Data from animals with similar ages were pooled and averaged. For statistical analysis, the thickness values at each P23H time point were compared with those of wild-type control animals of a similar age. Retinal thickness measurements were performed by two researchers independently, with very similar results.

In two animals, epithelium-attached slices were prepared. Thickness measurements from such retinal preparations did not yield different values from those in which the retina was separated from the epithelium and sclera.

Data processing and reporting

Multielectrode data were analyzed off-line using LabVIEW and IGOR Pro. Means and SEs were calculated in Excel; statistical tests were performed in IGOR Pro. Images were processed in Photoshop and Intaglio. Statistical significance was calculated by performing a nonparametric analysis (one- or two-tailed two-sample Wilcoxon–Mann–Whitney test) with a significance limit of $P < 0.05$.

Results are reported in the text as mean ± 1 SE, whereas the figure graphs show mean ± 1 SD.

The sigmoidal fit function in Fig. 2 is intended as a guide to the eye. A cumulative Gaussian (error function) was used

$$f(x) = c + aG(xb + d)$$

with

$$G(x) = \frac{2}{\sqrt{\pi}} \int_0^x e^{-t^2}\, dt$$

with the free parameters a, b, c, and d.

To compare rat and human ages, the following data were used (Quinn 2005): puberty at 50 days in the rat (11.5 yr in human), mature skeletal size at 210 days in the rat (20 yr in human), female reproductive senescence at 600 days (51 yr), and average life span of 2.5–3 yr (75–80 yr). Using pairwise linear interpolation between these time points, we calculated the following equivalent ages: P30 (rat) = 7 yr (human), P150 = 17 yr, P500 = 43 yr, P600 = 51 yr, P750 = 60 yr.

RESULTS

To assess the viability of degenerated retina for treatment with epiretinal prosthetic devices, we compared the anatomic structure and responses to visual and focal electrical stimulation in degenerated and control rat retinas over the first 2 years of postnatal life.

Animal species, strains, and ages

Retinas from transgenic P23H rats were compared with those of wild-type LE rats. To ensure that any differences between transgenic and wild-type animals were not attributable to their genetic background, the P23H mutation (originally in albino rats) was back-bred onto a pigmented LE background. This manipulation had the additional advantage that pigmented retinas more closely resemble retinas in typical cases of human degeneration. A total of 25 control (LE) animals and 30 P23H animals were used for this study, aged P30 (early life) to P750 (late mature adulthood). Limited data from a different retinal degeneration rat model (S334Ter) were included in some analyses (three animals). An additional 26 P23H rats were used for measurements of retinal thickness only.

Loss of photoreceptors during degeneration

To confirm retinal degeneration in P23H rats, retinas were fixed, stained, and inspected in cross section. Figure 1*A* shows examples at several postnatal ages. The healthy retina of an older rat (*top*) is compared with three P23H retinas. The young postnatal day P88 retina resembled that of the control rat, although some thinning of the outer retina had occurred. By P276 (9 mo), the outer segments of photoreceptors and the outer nuclear layer of P23H retinas had largely disappeared. The inner retina, however, appeared intact and formed the bulk of the remaining retinal thickness. At P663 (22 mo), further thinning had occurred and pigment epithelium granules were observed throughout the inner retina.

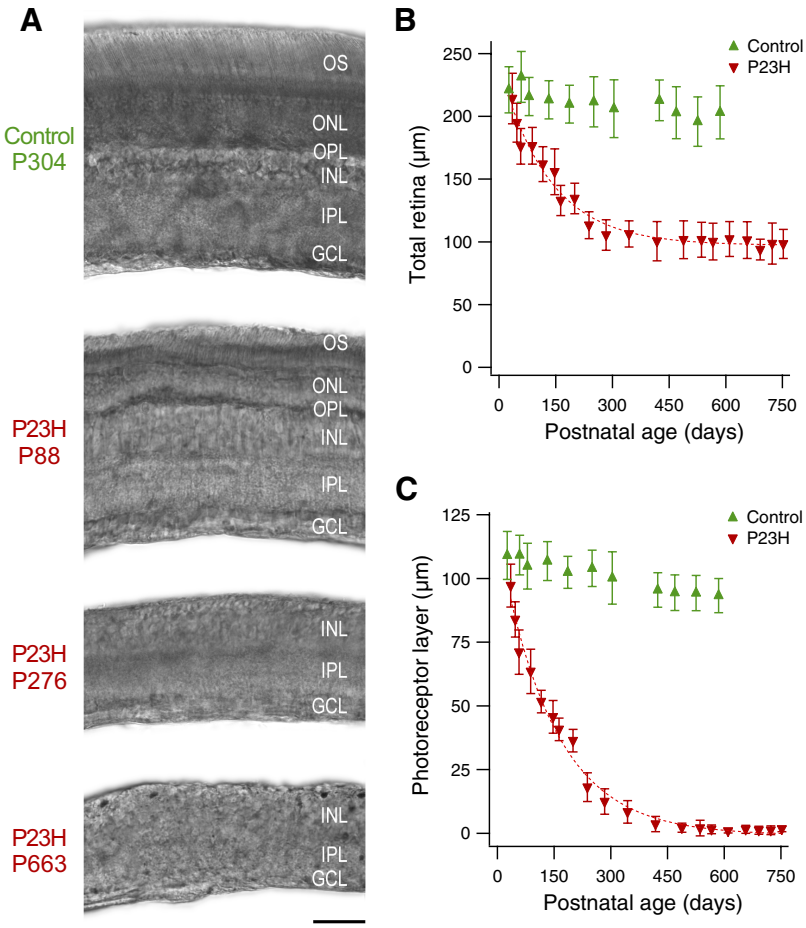

FIG. 1. Retinal thickness in normal and degenerated retina. *A*: representative examples of retinal cross sections in normal control and P23H rats. Degenerated retinas are shown at 3 different ages. The nearly complete loss of photoreceptor outer segments (OS), outer nuclear layer (ONL), and outer plexiform layer (OPL) was apparent by P276, whereas the inner nuclear layer (INL), inner plexiform layer (IPL), and ganglion cell layer (GCL) were less affected. Scale bar: 50 μm. *B*: thickness of the entire retina as a function of age. In control animals (green symbols), little change was observed, whereas P23H rats (red symbols) showed a decline in the first year of postnatal life. Each data point is an average of thickness measurements in 15–53 retinal cross sections from 1 to 3 animals. Dashed line is an exponential fit to the P23H data (τ = 132 days). Error bars: SD. *C*: thickness of the photoreceptor layer (ONL, inner and outer segments) as a function of age. Dashed line is an exponential fit to the P23H data (τ = 146 days). Error bars: SD.

The thickness of the retina was measured to assess cell loss during degeneration. Figure 1*B* shows retinal thickness as a function of age. Progressive retinal thinning occurred during the first 500 postnatal days in P23H animals, whereas LE retinas showed only a modest decrease in thickness. No further thinning was seen after P500. P23H retinas were significantly thinner ($P < 10^{-9}$) than wild-type controls at all ages except the lowest (P35, $P = 0.12$).

Figure 1*C* shows measurements of photoreceptor layer thickness. At each age, P23H retinas had significantly thinner photoreceptor layers ($P < 10^{-5}$). The time course of total retina and photoreceptor layer thinning was comparable in P23H animals (time constants 132 and 146 days, respectively), suggesting that the reduction in overall retinal thickness was largely accounted for by the loss of photoreceptors.

To investigate the possibility of differential effects of degeneration at different eccentricities, central and peripheral locations were analyzed separately. At all ages, retinal thickness was consistently greater at central locations by 18 ± 3 μm in control and 14 ± 1 μm in P23H animals. This difference appeared to primarily reflect differences in the inner retina because the thickness difference of the photoreceptor layer between central and peripheral locations was negligible (2 ± 1 μm). Central and peripheral locations showed a nearly identical time course of photoreceptor loss (τ = 147 and 144 days, respectively), suggesting a spatially uniform pattern of degeneration, at least on a macroscopic level.

In summary, pigmented P23H rats undergo slow but complete photoreceptor degeneration that results in a twofold thinning of the retina over the first 1.5 yr of postnatal life.

Ganglion cell physiology and light responses

During and following photoreceptor degeneration, the remainder of the retina reorganizes and remodels (Marc and Jones 2003). To assess the functional state of the retina during regeneration, action potentials were recorded from ganglion cells using a multielectrode array (MEA) with 61 electrodes. First, spontaneous and light-evoked firing was used to estimate the number of functional ganglion cells in each retina. In normal rat retina, MEA recordings typically yielded 40–50 unique recorded ganglion cells (see METHODS). We recorded a total of 1,136 cells in P23H and 1,131 cells in control animals. Figure 2*A* shows that in P23H retinas, similar cell counts were obtained during the first ~550 days as in control retinas. At ages >P550, however, P23H animals showed significantly fewer cells than those at ages <P550 ($P < 0.0001$). Recorded ganglion cell counts at higher ages stabilized at around half of those found in young retinas.

Second, we assessed responses to light. Retinas were stimulated using a white noise stimulus that revealed light-responsive ganglion cells in each retinal preparation. In typical control rat retina, about 90% of recorded ganglion cells responded to this stimulus. Figure 2*B* plots the percentage of light-responsive cells in normal rats and in P23H animals

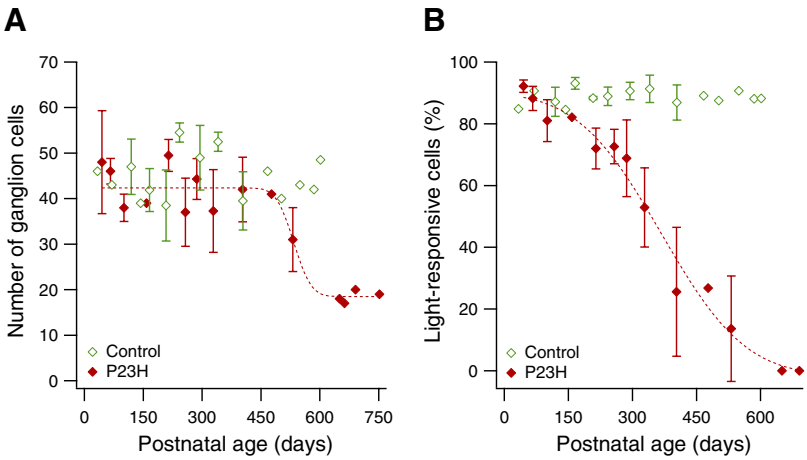

FIG. 2. Ganglion cell physiology in normal and degenerated retina. *A*: total number of recorded ganglion cells as a function of animal age. Each data point represents the average of 1–3 retinas and includes light-sensitive cells as well as cells not responsive to visual stimulation. Open symbols: normal control animals; closed symbols: P23H transgenic animals. The dashed line is a sigmoidal fit to the P23H data. Data points without error bars represent a single retina. *B*: percentage of recorded ganglion cells with light responses, plotted against the age of the animal. The dashed line is a sigmoidal fit to the P23H data.

during degeneration. In P23H retina, light responses were initially intact and indistinguishable from controls but, with advancing age, fewer cells exhibited visually evoked activity. By about P600, none of the recorded ganglion cells responded to the stimulus.

Thus although P23H retinas exhibited a decline in the number of physiologically active ganglion cells compared with control retinas, the decline in light responses was more rapid and complete.

Spontaneous firing

Ganglion cells in other animal models of retinal degeneration exhibit periods of vigorous hyperactivity (Dräger and Hubel 1978; Margolis et al. 2008; Sauve et al. 2001; Stasheff 2008). Spontaneous firing of P23H ganglion cells in the absence of visual stimuli was higher than that in control retinas. Figure 3*A* shows representative examples from animals of similar age, in which P23H cells fired four times as frequently as control cells. The average firing rate as a function of age is shown in Fig. 3*B*, for 212 P23H and 189 control cells. Control retinas exhibited average spontaneous firing rates of about 8 Hz, whereas two- and threefold higher firing rates were found in P23H retinas after P150. Hyperactivity was sustained for most of the age range studied, but firing rates returned to near control levels around P600–P650. Firing rates were significantly higher in P23H animals ($P < 0.05$) except at the earliest time point (P45) and time points >P650. Rhythmic burst firing was observed in a subset of P23H cells (not shown).

The amplitude of spontaneous spikes was also compared as a rough indicator of ganglion cell health. As shown in Fig. 3*C* for the same set of cells as in Fig. 3*B*, there was no difference in spike amplitude between P23H and control cells ($P > 0.1$), suggesting that ganglion cells in P23H retina were as healthy as those in control retina.

Responses to electrical stimulation

The responses of ganglion cells to direct electrical stimulation were compared in degenerated retinas and control retinas. The MEA was used to inject current through one electrode and simultaneously record evoked spikes at a neighboring electrode. Previous work suggests that ganglion cells in severely degenerated retina may require higher current injections to reach threshold (e.g., Chen et al. 2006; Jensen and Rizzo 2008) and respond at longer latencies (e.g., O'Hearn et al. 2006). Combined visual and electrical stimulation was performed in 130 ganglion cells from P23H rats and 95 cells from LE rats.

Near threshold, ganglion cells in both experimental groups responded to an electrical stimulus pulse with a single evoked spike at submillisecond latency (Fig. 4*A*). Threshold was de-

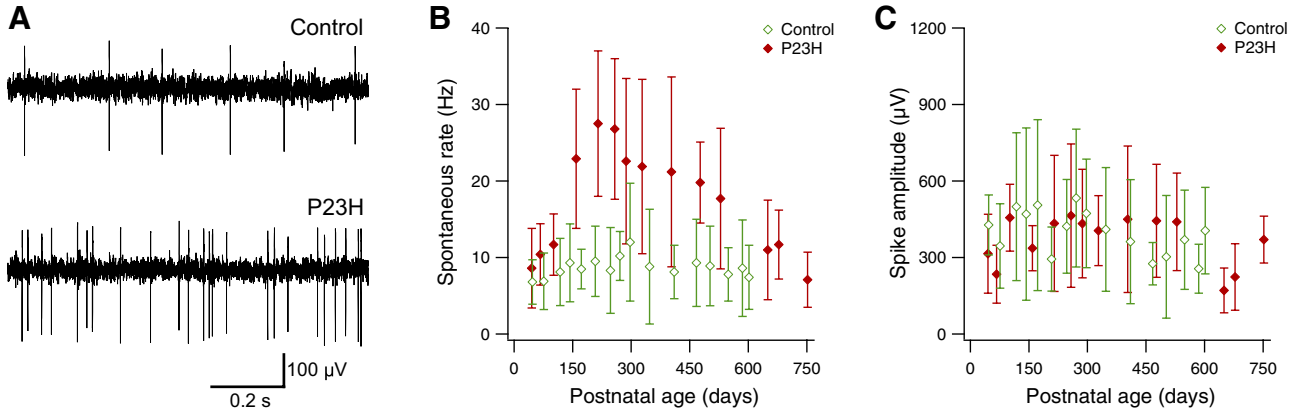

FIG. 3. Spontaneous ganglion cell activity in normal and P23H retina. *A*: examples of 1-s recordings of spontaneous activity in ganglion cells from a control (P247) and a P23H rat retina (P251). The P23H cell fired at >4 times the rate of the cell in the control group (24 and 6 Hz, respectively). *B*: spontaneous firing rate measured in 189 ganglion cells of control retina and 212 P23H cells as a function of animal age. Each data point represents the average rate measured in several cells from animals of similar age (12 ± 1 cells for control and 15 ± 2 cells for P23H). Error bars: SDs. *C*: amplitude of spontaneous spikes as a function of age in the same control and P23H animals as in *B*.

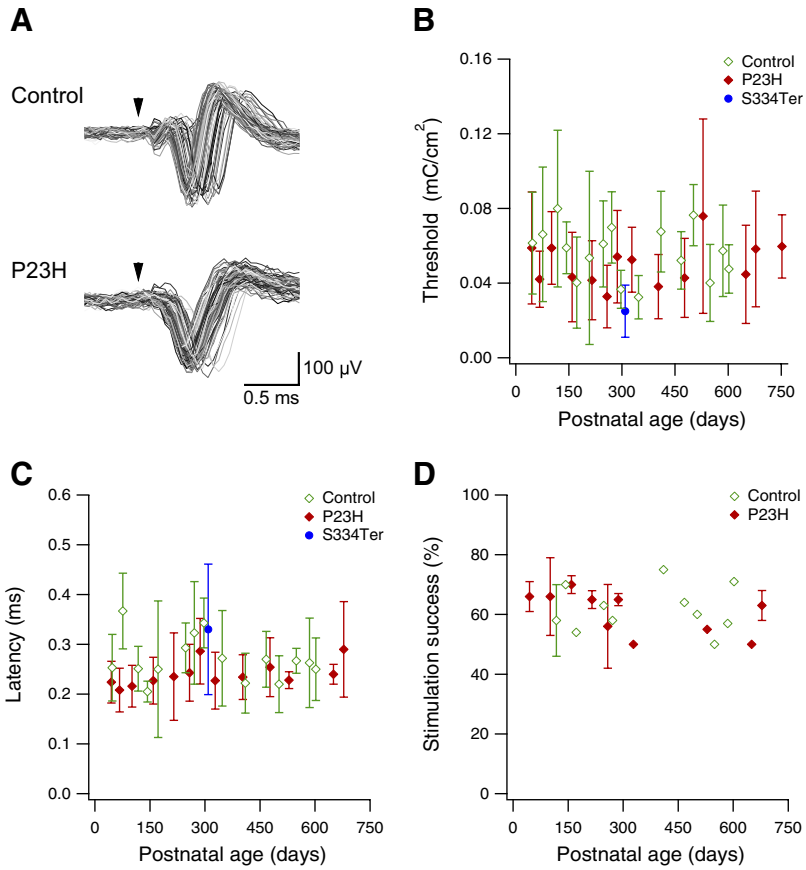

FIG. 4. Evoked spikes in normal and degenerated retina. *A*: examples of responses to 90 stimulation pulses (0.05-ms duration) near threshold in the same control and P23H cells shown in Fig. 3*A*. The stimulation artifact was subtracted digitally (see METHODS); the arrowhead indicates pulse onset. The control and P23H cells had thresholds of 0.06 and 0.05 mC/cm^2, respectively. *B*: charge density required to reach threshold (50% probability of evoking a spike) as a function of animal age. Each data point represents thresholds measured in 3–16 cells of 1–3 animals. Error bars: SDs. Data from 3 rats of the S334Ter line are shown in blue. Pulse durations were 0.05 or 0.1 ms. *C*: latency of evoked spikes for the same groups of animals. Only responses to 0.05-ms pulses were evaluated. *D*: success rate of stimulation in control and P23H retinas. This parameter was measured in only a subset of experiments, thus fewer data were available. Data points without error bars represent a single retina.

termined as the current that produced a response on 50% of pulses (see METHODS). The resulting thresholds are shown in Fig. 4*B*, expressed as charge density. Averaged across all age groups, P23H cells required 0.049 ± 0.002 mC/cm^2 to reach threshold (n = 130), whereas cells in wild-type retinas required 0.058 ± 0.003 mC/cm^2 (n = 95). Further analysis revealed that P23H thresholds were not significantly higher than control thresholds ($P > 0.9$); in fact, thresholds were found to be lower in P23H cells than those in the control group ($P = 0.004$). No systematic variation with age was observed for thresholds in P23H cells.

Figure 4*B* also shows data from nine cells in three S334Ter-3 rats, a different transgenic model for outer retinal degeneration. These animals were examined at an age at which the outer retina has completely degenerated (P309) (Lowe et al. 2005; Sagdullaev et al. 2003). Again, no substantial difference from control cells was observed.

To test whether degeneration affected electrical response latency, the time between the onset of a 0.05-ms pulse and the evoked spike was measured. All ganglion cells responded at latencies <0.5 ms; the average latency for P23H cells was 0.24 ± 0.01 ms (n = 107) and for control cells was 0.27 ± 0.01 ms (n = 62). Figure 4*C* shows latencies of control, P23H, and S334Ter retinas versus age. Similar values were found in all three groups and P23H latencies were not significantly higher than those of control cells ($P > 0.9$).

To ascertain whether cells with electrically evoked spikes were less frequently encountered in degenerated retina, the success rate of stimulation (fraction of successfully stimulated cells in all stimulation attempts per retina) was measured. Figure 4*D* shows the success rate for the subset of experiments for which this measurement was made. The success rate was 62 ± 2% in P23H experiments (n = 22 animals) and 63 ± 3% for control experiments (n = 12 animals), with no significant difference between the two groups ($P > 0.6$). The fact that success rates were substantially below 100% probably reflects a combination of amplifier saturation and cases in which the stimulus artifact prevented the unambiguous detection of evoked responses (typically >0.1 mC/cm^2). The success rate was slightly higher than that reported for epiretinal stimulation in primate retina (Sekirnjak et al. 2008).

To confirm that spikes in ganglion cells were directly evoked, cadmium chloride (0.5 mM) was added to the perfusion solution to block synaptic transmission. Evoked spikes were not abolished in six of six cells in three control retinas and five of five cells in two P23H retinas (data not shown).

DISCUSSION

Using pigmented P23H rats and multielectrode recording and stimulation, we have shown that ganglion cells in degenerating retina remain responsive to focal direct electrical stimulation in spite of complete photoreceptor degeneration and loss of light responses.

P23H transgenic rat model of retinal degeneration

We chose to examine the P23H transgenic rat since this strain contains the same rhodopsin mutation found in 11–15% of autosomal dominant RP (ADRP) families of U.S. origin, constituting the largest proportion attributable to any single

mutation (Rosenfeld and Dryja 1995; Sung et al. 1991). Note, however, that ADRP represents only about 15% of all RP cases (Olsson et al. 1992).

The P23H rat carries a mutant mouse opsin gene (Olsson et al. 1992) in addition to the endogenous native opsin genes (Lewin et al. 1998; Steinberg et al. 1996) and undergoes progressive photoreceptor apoptosis very similar to human ADRP. Histopathological and electrophysiological studies have shown broad similarities between the human P23H mutation and P23H rat retinal degeneration (Machida et al. 2000). Importantly, degeneration occurs only after the retina has fully matured, providing an advantage over other animal models such as the widely studied rd1 mouse (Carter-Dawson et al. 1978). Moreover, degeneration in the P23H rat begins with photoreceptor cells, in contrast to the commonly used Royal College of Surgeons (RCS) rat, where degeneration is triggered by a defect in retinal pigment epithelium cells (Dowling and Sidman 1962). We used heterozygous P23H rats with a single copy of the mutant transgene to further emulate the human genetic condition of ADRP (Berson et al. 1991).

The observed loss of outer retina and preservation of inner retina confirms the descriptions in previous studies of albino P23H animals (e.g., Machida et al. 2000; Olsson et al. 1992). In the present study, structural evidence indicates that ganglion cells survive long after the loss of the entire photoreceptor layer; this was further confirmed by the observation that the number of functional ganglion cells remained unchanged until late in the degeneration process. In young P23H rats, the measured retinal and photoreceptor layer thickness is comparable to typical values reported for juvenile wild-type rats (Joly et al. 2006), but then declines over the course of months. In the retinas of older P23H rats, we frequently observed pigment deposition reminiscent of the "bone spicules" found in histopathological reports of RP patients (Li et al. 1995), indicating an advanced stage of the disease process.

Photoreceptor loss progressed somewhat more slowly than previously reported for the P23H-1 line in albino rats (Cuenca et al. 2004; LaVail et al. 2000; Machida et al. 2000). This may be explained by our use of the Long–Evans rat strain as genetic background because eye pigmentation can slow down the rate of degeneration in P23H lines and delay photoreceptor loss (Leonard et al. 2007; Lowe et al. 2005). Pigmented rat retinas also contain substantially higher levels of rhodopsin than those of albino retinas (Battelle and LaVail 1978), more closely resembling the situation in human retina (Leonard et al. 2007). In this study, the time course of photoreceptor layer thinning was slowed by a factor of about 1.5–1.6 compared with that reported for albino rats.

The number of recorded ganglion cells eventually decreased (>P600), probably marking the late stages of degeneration-induced retinal restructuring. In albino P23H-1 rats, an extended late phase of negative remodeling with onset around P370 was found (Jones et al. 2003), which would correspond to about P600 in the pigmented P23H rats used here using the above-cited slowing factor. This "phase 3" period is characterized by extensive neuronal cell death throughout the retina, migration of inner nuclear layer neurons into the ganglion cell layer, and rewiring of the remnant inner plexiform layer (Jones and Marc 2005). Although this seems to be the likeliest explanation for the decrease in functional cell numbers, a small contribution is expected to arise from "silent cells": a fraction of ganglion cells do not fire spontaneously in darkness but do fire in response to visual stimulation. Since older P23H retinas are essentially blind, silent cells would not be recorded under any condition. However, the effect is likely small: in five rat retinas, 6 ± 2% fewer ganglion cells were recorded under dark conditions compared with visual stimulation (unpublished observations).

Loss of light responses and preservation of ganglion cells

Not surprisingly, P23H retinas became less responsive to light stimulation as degeneration progressed. The drop in the fraction of light-responsive cells was not due to a reduced overall number of active ganglion cells, since cell counts did not differ between the two experimental groups until about P550. Rather, responsiveness to light apparently decreased as a consequence of photoreceptor loss.

The remaining light responses after about P300 may be mediated by cone photoreceptors. Consistent with this possibility, rd1 mouse rod degeneration precedes cone degeneration (Carter-Dawson et al. 1978). Anatomical evidence indicates that cones are also preserved in P23H rats until long after rods have completely degenerated (Chrysostomou et al. 2009). It has been reported that in homozygous P23H rats, cones appear to synapse onto both rod and cone bipolar cells after rods have degenerated (Cuenca et al. 2004). The rapid decrease in photoreceptor layer thickness with age (see Fig. 1*C*) may be due to loss of the longer rod outer segments, while enough cones could be preserved to give rise to a few light-responsive cells in animals as old as P500 (see Fig. 2*B*). It is indeed possible that a very sparse population of preserved cone photoreceptors escaped the thickness measurements.

In older P23H animals (>P300), there was considerable variability in the measurements of the number of light-responsive cells, evident as large SDs in Fig. 2*B*. We attribute this variance to nonhomogeneous photoreceptor degeneration across the retina, perhaps on a level of tens of microns. Although no direct evidence for patchy photoreceptor loss exists, degeneration is usually slightly more advanced in the superior hemisphere than that in the inferior hemisphere and there are central-to-peripheral gradients of degeneration (M. LaVail, personal communication).

Hyperactivity in degenerated retina

Ganglion cells in P23H retina showed a marked increase in spontaneous activity in the period during which photoreceptors degenerated. This observation is consistent with the hyperactivity reported in rd1 mouse ganglion cells (Margolis et al. 2008; Stasheff 2008), indirect evidence from superior colliculus recordings (Dräger and Hubel 1978; Sauve et al. 2001), and intracellular recordings in RCS rats (Pu et al. 2006). Whereas rd1 mouse retinas show rhythmic burst firing in every cell (Margolis et al. 2008), only a subset of cells in P23H retina appeared to display this behavior.

The origin of the observed hyperactivity is unknown. One possibility is a change in the intrinsic membrane properties that underlie spontaneous firing: loss of inputs might lead to increased excitability. Since ganglion cells in this study remained responsive to electrical stimulation in spite of elevated spontaneous activity, general cellular hyperexcitability (such as a

higher resting membrane potential) does not seem to provide a satisfactory explanation. Alternatively, degeneration-induced changes to the retinal circuitry may be the source of hyperactivity. Reorganization of bipolar and amacrine cell connectivity could result in an altered balance of excitatory and inhibitory inputs to ganglion cells (Stasheff 2008). An increase in glutamate signaling has been demonstrated in degenerated retina (Marc et al. 2007) and the resting currents of voltage-clamped ganglion cells in rd1 mice show substantial reductions when synaptic antagonists are applied (Margolis et al. 2008). It would be telling to block synaptic transmission in P23H retina during the period of elevated spontaneous firing to examine the contribution of synaptic drive to hyperactivity.

Remarkably, at advanced ages (~P600) spontaneous rates approach those of control animals. Previous studies have not reported this observation, possibly because they did not include the latest phase of degeneration.

Thresholds for focal direct electrical stimulation

By combining short stimulation pulses (0.05–0.1 ms), small stimulation electrodes (10–15 μm), and low current amplitudes (<5 μA), we ensured that current spread was limited so that only ganglion cells near the stimulation site were activated. The observed submillisecond stimulus-locked spikes and their resistance to block of synaptic transmission confirmed direct activation.

Thresholds in the present study are comparable to those reported in primate retina using the same stimulation methods, with charge densities around 0.05 mC/cm^2 (Sekirnjak et al. 2008). Similar thresholds have also been reported for epiretinal stimulation of frog retina with 40-μm disk electrodes (Kuras et al. 2004) and rabbit retina with 30-μm cone-shaped electrodes (Fried et al. 2006). Thresholds were consistently within the established electrochemical safety limits for platinum electrodes (between 0.1 and 0.4 mC/cm^2; Brummer and Turner 1977; Rose and Robblee 1990). The data exhibited some variability, which is likely explained by variations in the location of the stimulation electrode relative to the target cell, in particular relative to the axon (Fried et al. 2009; Sekirnjak et al. 2008). This variability is inherent to our stimulation technique and is comparable to that seen in our previous studies (Sekirnjak et al. 2006, 2008).

The present results indicate that when ganglion cells are directly activated using small electrodes and short pulses, stimulation thresholds in control and degenerated retina are similar. This finding stands in apparent contrast with previous work. Degenerated rabbit retina showed thresholds 1.3 times those of normal rabbit retina when stimulated with 200-μm electrodes (Humayun et al. 1994). A report of epiretinal stimulation with 254-μm electrodes in rd1 mice found a doubling of thresholds and pointed toward bipolar cells as the site of stimulation (Katona et al. 1998), while subretinal stimulation with 400-μm electrodes resulted in 7.4-fold higher thresholds (Jensen and Rizzo 2009). A number of studies using 125-μm electrodes in rd1 mice reported higher thresholds than those found in normal mouse retina: 1.2–1.6 times (Suzuki et al. 2004), 2.3 times (Chen et al. 2006), and a strong trend toward higher thresholds (O'Hearn et al. 2006). Preliminary results from three normal and four rd1 ganglion cells yielded twofold higher thresholds for degenerated retina using 30-μm electrodes and 0.06-ms pulses; however, the authors were unable to confirm that the earliest spikes (2- to 3-ms latency) were due to direct activation (Ye et al. 2008). Severely degenerated S334Ter rats showed significantly higher thresholds when stimulated with 75-μm electrodes and recorded in the superior colliculus (Chan et al. 2008). In human RP patients, the thresholds for epiretinal stimulation with 400-μm electrodes and 2-ms pulses were 7- to 10-fold compared with a normally sighted volunteer (Rizzo et al. 2003). Similarly, areas of more severe damage within the retinas of RP patients had higher electrical thresholds for stimulation with 125-μm electrodes and 1- to 2-ms pulses (Humayun et al. 1999).

However, all of the previous studies almost certainly activated cells other than ganglion cells, producing complex interactions in the degenerating retinal circuitry, and thus essentially reported the aggregated response of ganglion and nonganglion cell types to electrical pulses. It is well known that the use of large electrodes and/or long pulse durations will predominantly target deeper retinal neurons such as bipolar cells and photoreceptors (Fried et al. 2006; Greenberg et al. 1998; Jensen and Rizzo 2007; Margalit and Thoreson 2006; Sekirnjak et al. 2006; Ziv et al. 2002). The reported long latencies of spike responses (2–20 ms) and the absence of single, time-locked action potentials are characteristic indications of presynaptic cell activation rather than direct stimulation. During degeneration, second-order retinal cells undergo massive remodeling, regression of dendrites, and cell death, whereas ganglion cells are relatively spared (Jones et al. 2003). A recent study reports that in rd10 mice, ganglion cells retain their morphology, fine dendritic geometry, and cell density well beyond the complete death of photoreceptors (Mazzoni et al. 2008), whereas in the same retinas bipolar and horizontal cells undergo regressive remodeling (Gargini et al. 2007). Moreover, a report in rd1 mice highlights the functional stability of ganglion cells during retinal disease and concludes that intrinsic firing properties of ganglion cells remained essentially intact (Margolis et al. 2008).

The present study shows that directly evoked spiking in ganglion cells is not compromised, even in tissue with late-stage degeneration. This conclusion is supported by the finding that perceptual thresholds with optic nerve stimulation in RP patients are similar to those in normal patients (Veraart et al. 1998) and has promising implications for the design of retinal prostheses (see below).

Implications

Validation of the P23H animal model of RP. The P23H rat was recently shown to support implantation of inactive prototype implants (Salzmann et al. 2006) and can provide a suitable model to study the long-term stimulation of dystrophic retina. Furthermore, when rat ages are converted to human ages (see METHODS), a disease progression time course very similar to that of human RP emerges (Berson et al. 1991; Tsujikawa et al. 2008). Finally, degeneration occurs only after the retina is fully developed in both the P23H model and human RP. Although there are many causes of retinal degeneration in humans, the pigmented P23H rat emerges as a valuable animal model that closely mimics the diseased state of advanced ADRP.

Human retinal implants. Responsiveness of ganglion cells to direct focal electrical stimulation in late-stage degenerated

retina is a prerequisite for the development of high-resolution human implants. The present results therefore suggest several implications for future prosthetic devices. First, the low thresholds found here indicate that ganglion cells retain their responsiveness to epiretinal stimulation even in severely degenerated retina that contains fewer ganglion cells. Second, our results support the epiretinal approach for implementing a high-resolution device, since the implant would be able to bypass much of the diseased outer retinal circuitry and drive inner retinal cells directly, and since an array positioned at the epiretinal surface should have the proximity required for stimulation of ganglion cells.

In conclusion, our results indicate that the ganglion cell population presents an attractive target for focal direct electrical activation in retinas affected by diseases such as RP.

ACKNOWLEDGMENTS

We thank M. LaVail and Chrysalis DNX Transgenic Sciences (Princeton, NJ) for providing the P23H breeding animals and J. Weiland for the S334Ter rats.

GRANTS

This research was supported by the Salk Institute Pioneer Postdoctoral Fellowship, Second Sight Medical Products Inc. (SSMP), NEI grants EY-018003 (E. J. Chichilnisky) and EY-012893 (SSMP), NSF grant PHY-0417175 and NIH grant R21EB-004410 (A. M. Litke), the Burroughs Wellcome Fund Career Award at Scientific Interfaces (A. Sher), and the Polish Ministry of Science Higher Education (W. Dabrowski).

REFERENCES

Battelle BA, LaVail MM. Rhodopsin content and rod outer segment length in albino rat eyes: modification by dark adaptation. *Exp Eye Res* 26: 487–497, 1978.

Berson EL, Rosner B, Sandberg MA, Dryja TP. Ocular findings in patients with autosomal dominant retinitis pigmentosa and a rhodopsin gene defect (Pro-23-His). *Arch Ophthalmol* 109: 92–101, 1991.

Brummer SB, Turner MJ. Electrical stimulation with Pt electrodes: II. Estimation of maximum surface redox (theoretical non-gassing) limits. *IEEE Trans Biomed Eng* 24: 440–443, 1977.

Carter-Dawson LD, LaVail MM, Sidman RL. Differential effect of the rd mutation on rods and cones in the mouse retina. *Invest Ophthalmol Vis Sci* 17: 489–498, 1978.

Chan LH, Ray A, Thomas BB, Humayun MS, Weiland JD. In vivo study of response threshold in retinal degenerate model at different degenerate stages. *30th Annu Int Conf Proc IEEE Eng Med Biol Soc* August 20–24, 2008, Vancouver, BC, Canada.

Chen SJ, Mahadevappa M, Roizenblatt R, Weiland J, Humayun M. Neural responses elicited by electrical stimulation of the retina. *Trans Am Ophthalmol Soc* 104: 252–259, 2006.

Chichilnisky EJ. A simple white noise analysis of neuronal light responses. *Network* 12: 199–213, 2001.

Chrysostomou V, Stone J, Valter K. Life history of cones in the rhodopsin-mutant P23H-3 rat: evidence of long-term survival. *Invest Ophthalmol Vis Sci* 50: 2407–2416, 2009.

Cuenca N, Pinilla I, Sauve Y, Lu B, Wang S, Lund RD. Regressive and reactive changes in the connectivity patterns of rod and cone pathways of P23H transgenic rat retina. *Neuroscience* 127: 301–317, 2004.

Dabrowski W, Grybos P, Hottowy P, Skoczen A, Swientek K, Grillo AA, Kachiguine S, Litke AM, Sher A. Development of front-end ASICs for imaging neuronal activity in live tissue. *Nucl Instrum Methods Phys Res A* 541: 405–411, 2005.

Dowling JE, Sidman RL. Inherited retinal dystrophy in the rat. *J Cell Biol* 14: 73–109, 1962.

Dräger UC, Hubel DH. Studies of visual function and its decay in mice with hereditary retinal degeneration. *J Comp Neurol* 180: 85–114, 1978.

Fried SI, Hsueh HA, Werblin FS. A method for generating precise temporal patterns of retinal spiking using prosthetic stimulation. *J Neurophysiol* 95: 970–978, 2006.

Fried SI, Lasker AC, Desai NJ, Eddington DK, Rizzo JF. Axonal sodium-channel bands shape the response to electric stimulation in retinal ganglion cells. *J Neurophysiol* 101: 1972–1987, 2009.

Gargini C, Terzibasi E, Mazzoni F, Strettoi E. Retinal organization in the retinal degeneration 10 (rd10) mutant mouse: a morphological and ERG study. *J Comp Neurol* 500: 222–238, 2007.

Greenberg R, Humayun M, de Juan E Jr. Different cellular time constants allows selective electrical stimulation of retinal neurons (Abstract). *Invest Ophthalmol Vis Sci* 39: S903, 1998.

Humayun MS, de Juan E Jr, Weiland JD, Dagnelie G, Katona S, Greenberg R, Suzuki S. Pattern electrical stimulation of the human retina. *Vision Res* 39: 2569–2576, 1999.

Humayun MS, Propst R, de Juan E Jr, McCormick K, Hickingbotham D. Bipolar surface electrical stimulation of the vertebrate retina. *Arch Ophthalmol* 112: 110–116, 1994.

Javaheri M, Hahn DS, Lakhanpal RR, Weiland JD, Humayun MS. Retinal prostheses for the blind. *Ann Acad Med Singapore* 35: 137–144, 2006.

Jensen RJ, Rizzo JF. Responses of ganglion cells to repetitive electrical stimulation of the retina. *J Neural Eng* 4: S1–S6, 2007.

Jensen RJ, Rizzo JF. Activation of retinal ganglion cells in wild-type and rd1 mice through electrical stimulation of the retinal neural network. *Vision Res* 48: 1562–1568, 2008.

Jensen RJ, Rizzo JF. Activation of ganglion cells in wild-type and *rd1* mouse retinas with monophasic and biphasic current pulses. *J Neural Eng* 6:035004 (May 20, 2009).

Jensen RJ, Rizzo JF, Ziv OR, Grumet A, Wyatt J. Thresholds for activation of rabbit retinal ganglion cells with an ultrafine, extracellular microelectrode. *Invest Ophthalmol Vis Sci* 44: 3533–3543, 2003.

Joly S, Pernet V, Dorfman AL, Chemtob S, Lachapelle P. Light-induced retinopathy: comparing adult and juvenile rats. *Invest Ophthalmol Vis Sci* 47: 3202–3212, 2006.

Jones BW, Marc RE. Retinal remodeling during retinal degeneration. *Exp Eye Res* 81: 123–137, 2005.

Jones BW, Watt CB, Frederick JM, Baehr W, Chen CK, Levine EM, Milam AH, Lavail MM, Marc RE. Retinal remodeling triggered by photoreceptor degenerations. *J Comp Neurol* 464: 1–16, 2003.

Katona SJ, Humayun MS, de Juan E Jr, Suzuki S, Weiland JD, Greenberg R. A comparison of electrical stimulation thresholds in normal versus degenerated (rd) mouse retina (Abstract). *Invest Ophthalmol Vis Sci* 39: S991, 1998.

Kuras A, Baginskas A, Batuleviciene V. Suprathreshold excitation of frog tectal neurons by short spike trains of single retinal ganglion cell. *Exp Brain Res* 159: 509–518, 2004.

LaVail MM, Yasumura D, Matthes MT, Drenser KA, Flannery JG, Lewin AS, Hauswirth WW. Ribozyme rescue of photoreceptor cells in P23H transgenic rats: long-term survival and late-stage therapy. *Proc Natl Acad Sci USA* 97: 11488–11493, 2000.

Leonard KC, Petrin D, Coupland SG, Baker AN, Leonard BC, LaCasse EC, Hauswirth WW, Korneluk RG, Tsilfidis C. XIAP protection of photoreceptors in animal models of retinitis pigmentosa. *PLoS ONE* 2: e314, 2007.

Lewin AS, Drenser KA, Hauswirth WW, Nishikawa S, Yasumura D, Flannery JG, LaVail MM. Ribozyme rescue of photoreceptor cells in a transgenic rat model of autosomal dominant retinitis pigmentosa. *Nat Med* 4: 967–971, 1998.

Li ZY, Possin DE, Milam AH. Histopathology of bone spicule pigmentation in retinitis pigmentosa. *Ophthalmology* 102: 805–816, 1995.

Litke AM. The retinal readout system: an application of microstrip detector technology to neurobiology. *Nucl Instrum Methods Phys Res A* 418: 203–209, 1998.

Litke AM, Bezayiff N, Chichilnisky EJ, Cunningham W, Dabrowski W, Grillo AA, Grivich M, Grybos P, Hottowy P, Kachiguine S, Kalmar RS, Mathieson K, Petrusca D, Rahman M, Sher A. What does the eye tell the brain? Development of a system for the large scale recording of retinal output activity. *IEEE Trans Nucl Sci* 51: 1434–11440, 2004.

Litke AM, Chichilnisky EJ, Dabrowski W, Grillo AA, Grybos P, Kachiguine S, Rahman M, Taylor G. Large-scale imaging of retinal output activity. *Nucl Instrum Methods Phys Res A* 501: 298–307, 2003.

Lowe RJ, Duncan JL, Yang H, Donohue-Rolfe KM, Matthes MT, Yasumura D, LaVail MM. Retinal degeneration is slowed by eye pigmentation in P23H but not in S334ter mutant rhodopsin transgenic rats. *Invest Ophthalmol Vis Sci* 46: ARVO Abstract 2300, 2005.

Machida S, Kondo M, Jamison JA, Khan NW, Kononen LT, Sugawara T, Bush RA, Sieving PA. P23H rhodopsin transgenic rat: correlation of retinal

function with histopathology. *Invest Ophthalmol Vis Sci* 41: 3200–3209, 2000.

Mahadevappa M, Weiland JD, Yanai D, Fine I, Greenberg RJ, Humayun MS. Perceptual thresholds and electrode impedance in three retinal prosthesis subjects. *IEEE Trans Neural Syst Rehabil Eng* 13: 201–206, 2005.

Marc RE, Jones BW. Retinal remodeling in inherited photoreceptor degenerations. *Mol Neurobiol* 28: 139–147, 2003.

Marc RE, Jones BW, Anderson JR, Kinard K, Marshak DW, Wilson JH, Wensel T, Lucas RJ. Neural reprogramming in retinal degeneration. *Invest Ophthalmol Vis Sci* 48: 3364–3371, 2007.

Margalit E, Thoreson WB. Inner retinal mechanisms engaged by retinal electrical stimulation. *Invest Ophthalmol Vis Sci* 47: 2606–2612, 2006.

Margolis DJ, Newkirk G, Euler T, Detwiler PB. Functional stability of retinal ganglion cells after degeneration-induced changes in synaptic input. *J Neurosci* 28: 6526–6536, 2008.

Mazzoni F, Novelli E, Strettoi E. Retinal ganglion cells survive and maintain normal dendritic morphology in a mouse model of inherited photoreceptor degeneration. *J Neurosci* 28: 14282–14292, 2008.

Mendez A, Burns ME, Roca A, Lem J, Wu LW, Simon MI, Baylor DA, Chen J. Rapid and reproducible deactivation of rhodopsin requires multiple phosphorylation sites. *Neuron* 28: 153–164, 2000.

Mokwa W, Goertz M, Koch C, Krisch I, Trieu HK, Walter P. Intraocular epiretinal prosthesis to restore vision in blind humans. *Conf Proc IEEE Eng Med Biol Soc* 2008: 5790–5793, 2008.

O'Hearn TM, Sadda SR, Weiland JD, Maia M, Margalit E, Humayun MS. Electrical stimulation in normal and retinal degeneration (rd1) isolated mouse retina. *Vision Res* 46: 3198–3204, 2006.

Olsson JE, Gordon JW, Pawlyk BS, Roof D, Hayes A, Molday RS, Mukai S, Cowley GS, Berson EL, Dryja TP. Transgenic mice with a rhodopsin mutation (Pro23His): a mouse model of autosomal dominant retinitis pigmentosa. *Neuron* 9: 815–830, 1992.

Pu M, Xu L, Zhang H. Visual response properties of retinal ganglion cells in the Royal College of Surgeons dystrophic rat. *Invest Ophthalmol Vis Sci* 47: 3579–3585, 2006.

Quinn R. Comparing rat's to human's age: how old is my rat in people years? *Nutrition* 21: 775–777, 2005.

Rizzo JF, Wyatt J, Loewenstein J, Kelly S, Shire D. Methods and perceptual thresholds for short-term electrical stimulation of human retina with microelectrode arrays. *Invest Ophthalmol Vis Sci* 44: 5355–5361, 2003.

Rose TL, Robblee LS. Electrical stimulation with Pt electrodes. VIII. Electrochemically safe charge injection limits with 0.2 ms pulses. *IEEE Trans Biomed Eng* 37: 1118–1120, 1990.

Rosenfeld PJ, Dryja TP. Molecular genetics of retinitis pigmentosa and related retinal degenerations. In: *Molecular Genetics of Ocular Disease*, edited by Wiggs JL. New York: Wiley–Liss, 1995, vol. 1, p. 99–126.

Sagdullaev BT, Aramant RB, Seiler MJ, Woch G, McCall MA. Retinal transplantation-induced recovery of retinotectal visual function in a rodent model of retinitis pigmentosa. *Invest Ophthalmol Vis Sci* 44: 1686–1695, 2003.

Salzmann J, Linderholm OP, Guyomard JL, Paques M, Simonutti M, Lecchi M, Sommerhalder J, Dubus E, Pelizzone M, Bertrand D, Sahel J, Renaud P, Safran AB, Picaud S. Subretinal electrode implantation in the P23H rat for chronic stimulations. *Br J Ophthalmol* 90: 1183–1187, 2006.

Sauve Y, Girman SV, Wang S, Lawrence JM, Lund RD. Progressive visual sensitivity loss in the Royal College of Surgeons rat: perimetric study in the superior colliculus. *Neuroscience* 103: 51–63, 2001.

Sekirnjak C, Hottowy P, Sher A, Dabrowski W, Litke AM, Chichilnisky EJ. Electrical stimulation of mammalian retinal ganglion cells with multielectrode arrays. *J Neurophysiol* 95: 3311–3327, 2006.

Sekirnjak C, Hottowy P, Sher A, Dabrowski W, Litke AM, Chichilnisky EJ. High-resolution electrical stimulation of primate retina for epiretinal implant design. *J Neurosci* 28: 4446–4456, 2008.

Shyu JS, Maia M, Weiland JD, Ohearn T, Chen SJ, Margalit E, Suzuki S, Humayun MS. Electrical stimulation in isolated rabbit retina. *IEEE Trans Neural Syst Rehabil Eng* 14: 290–298, 2006.

Stasheff SF. Emergence of sustained spontaneous hyperactivity and temporary preservation of OFF responses in ganglion cells of the retinal degeneration (rd1) mouse. *J Neurophysiol* 99: 1408–1421, 2008.

Steinberg RH, Flannery JG, Naash MI. Transgenic rat models of inherited retinal degeneration caused by mutant opsin genes (Abstract). *Invest Ophthalmol Vis Sci* 37: S698, 1996.

Sung CH, Davenport CM, Hennessey JC, Maumenee IH, Jacobson SG, Heckenlively JR, Nowakowski R, Fishman G, Gouras P, Nathans J. Rhodopsin mutations in autosomal dominant retinitis pigmentosa. *Proc Natl Acad Sci USA* 88: 6481–6485, 1991.

Suzuki S, Humayun MS, Weiland JD, Chen SJ, Margalit E, Piyathaisere DV, de Juan E Jr. Comparison of electrical stimulation thresholds in normal and retinal degenerated mouse retina. *Jpn J Ophthalmol* 48: 345–349, 2004.

Tsujikawa M, Wada Y, Sukegawa M, Sawa M, Gomi F, Nishida K, Tano Y. Age at onset curves of retinitis pigmentosa. *Arch Ophthalmol* 126: 337–340, 2008.

Veraart C, Raftopoulos C, Mortimer JT, Delbeke J, Pins D, Michaux G, Vanlierde A, Parrini S, Wanet-Defalque MC. Visual sensations produced by optic nerve stimulation using an implanted self-sizing spiral cuff electrode. *Brain Res* 813: 181–186, 1998.

Winter JO, Cogan SF, Rizzo JF. Retinal prostheses: current challenges and future outlook. *J Biomater Sci Polym Ed* 18: 1031–1055, 2007.

Yanai D, Weiland JD, Mahadevappa M, Greenberg RJ, Fine I, Humayun MS. Visual performance using a retinal prosthesis in three subjects with retinitis pigmentosa. *Am J Ophthalmol* 143: 820–827, 2007.

Ye JH, Kim KH, Goo YS. Comparison of electrically-evoked ganglion cell responses in normal and degenerate retina. *Conf Proc IEEE Eng Med Biol Soc* 2008: 2465–2468, 2008.

Ziv OR, Jensen RJ, Rizzo JF. In vitro activation of ganglion cells in rabbit retina: effects of glutamate receptor agents. *Invest Ophthalmol Vis Sci* 43: E-Abstract 4474, 2002.

Zrenner E, Wilke R, Bartz-Schmidt K, Benav H, Besch D, Gekeler F, Koch J, Porubská K, Sachs H, Wilhelm B. Blind retinitis pigmentosa patients can read letters and recognize the direction of fine stripe patterns with subretinal electronic implants. *Invest Ophthalmol Vis Sci* 50: E-Abstract 4581, 2009.